

1. **Studies of signal and background separation using Mann-Whitney U test and some new methods**

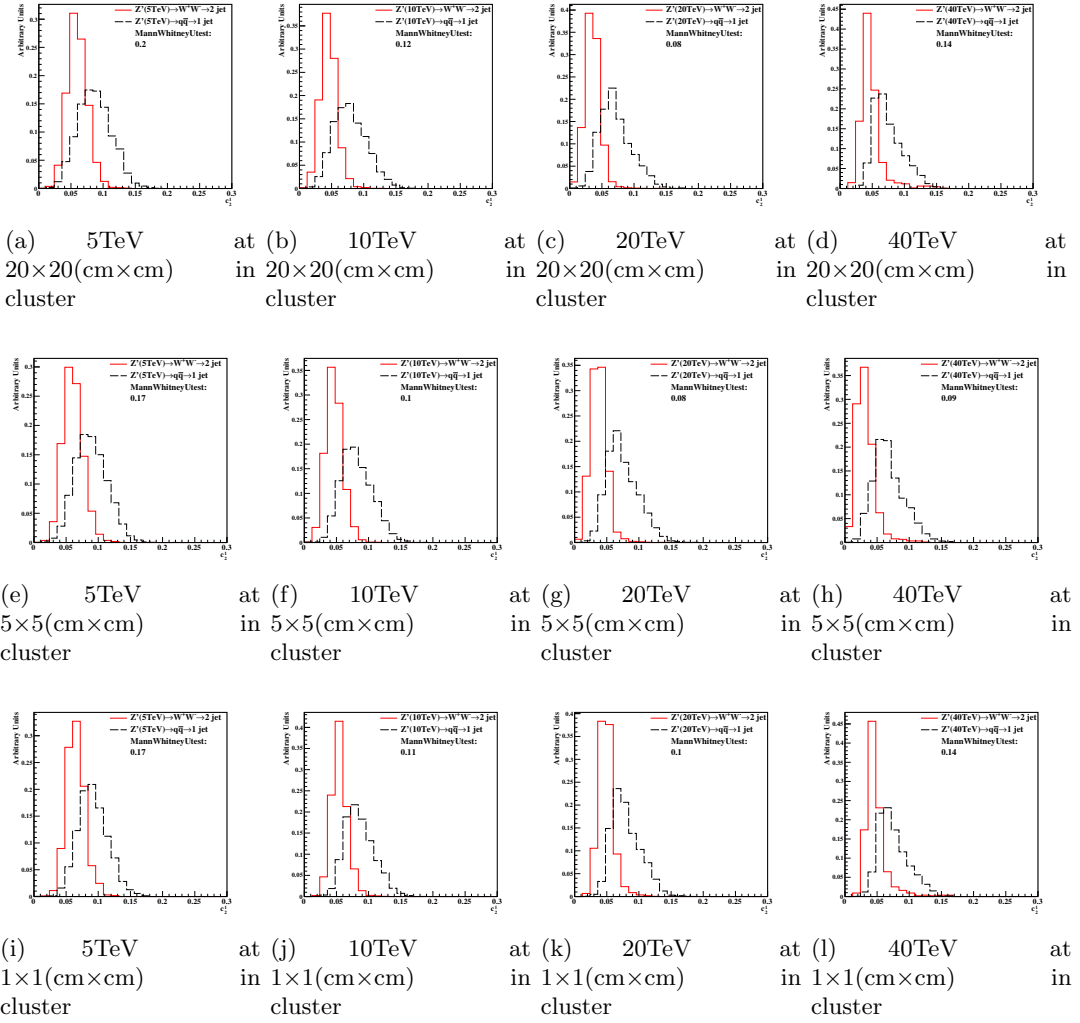
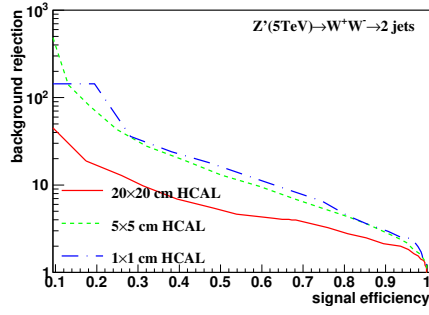
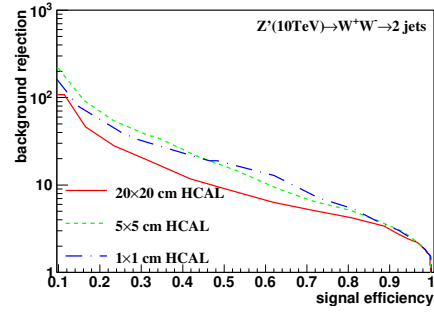


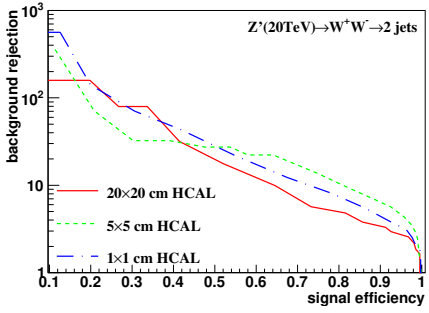
Figure 1: Distributions of Mann-Whitney value  $U$  in 5, 10, 20, 40 TeV energy collision for  $c_2^{(1)}$  in different detector sizes. Cell Size in  $20 \times 20$ ,  $5 \times 5$ , and  $1 \times 1 (\text{cm} \times \text{cm})$  are shown here.



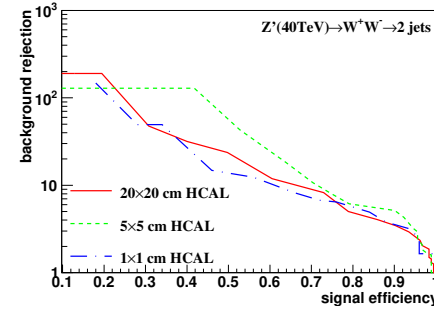
(a) 5 TeV using cluster method with New2 after cut Method



(b) 10 TeV using cluster method with New2 after cut Method



(c) 20 TeV using cluster method with New2 after cut Method



(d) 40 TeV using cluster method with New2 after cut Method

Figure 2: Signal efficiency versus background rejection rate using c2b1. The energies of collision at (a) 5, (b) 10, (c) 20, (d) 40 TeV are shown here. In each picture, the three ROC curves correspond to different detector sizes.

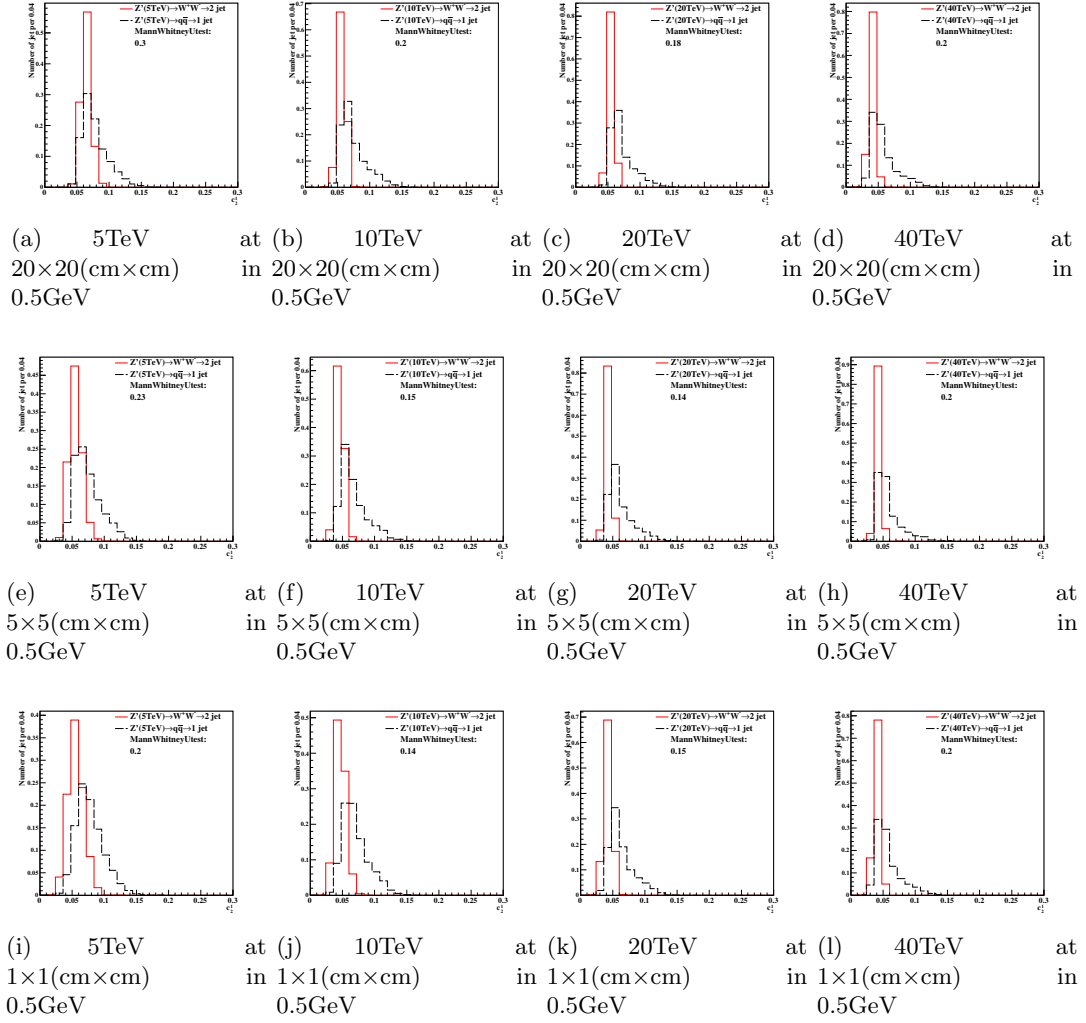
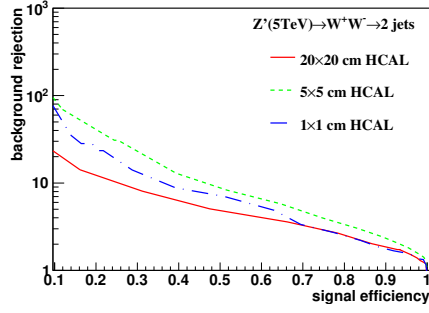
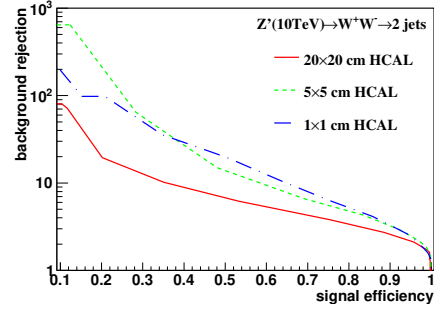


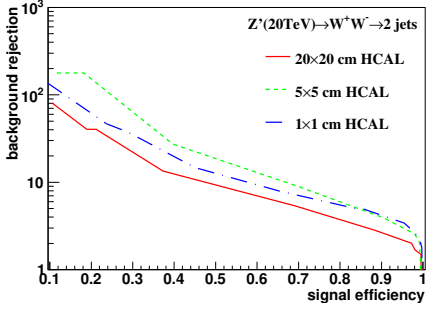
Figure 3: Distributions of Mann-Whitney value U in 5, 10, 20, 40TeV energy collision for c2b1 in different detector sizes. Cell Size in 20×20, 5×5, and 1×1(cm×cm) are shown here.



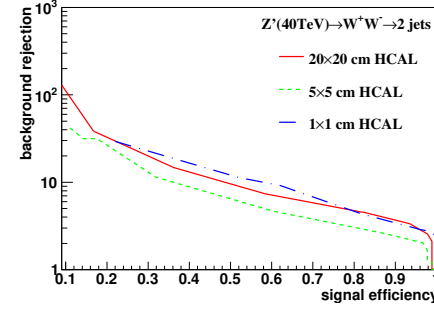
(a) 5 TeV using Rawhit 0.5GeV cut method with New2 after cut Method



(b) 10 TeV using Rawhit 0.5GeV cut method with New2 after cut Method



(c) 20 TeV using Rawhit 0.5GeV cut method with New2 after cut Method



(d) 40 TeV using Rawhit 0.5GeV cut method with New2 after cut Method

Figure 4: Signal efficiency versus background rejection rate using c2b1. The energies of collision at (a)5, (b)10, (c)20, (d)40TeV are shown here. In each picture, the three ROC curves correspond to different detector sizes.

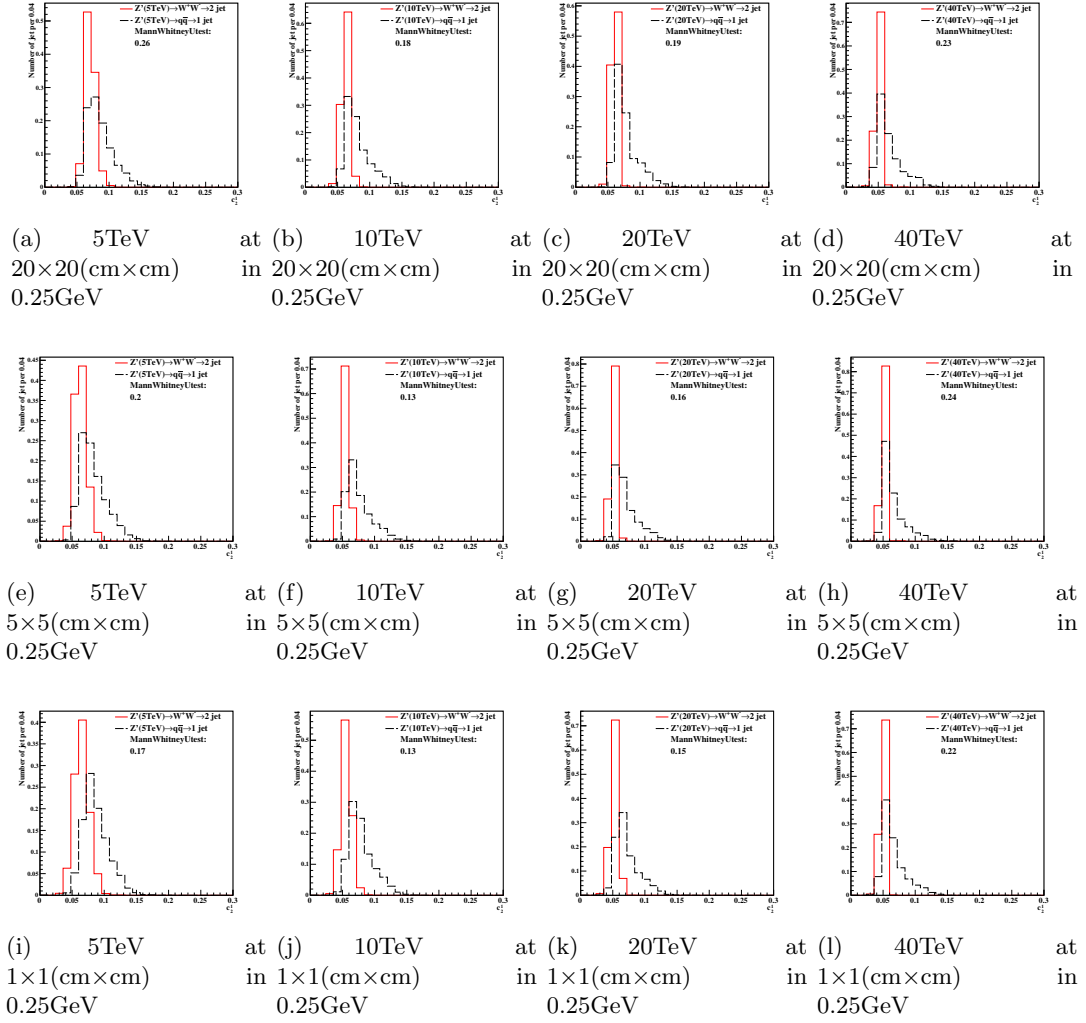
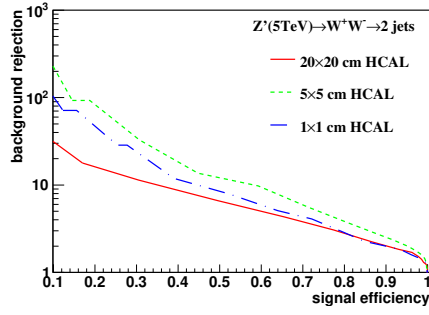
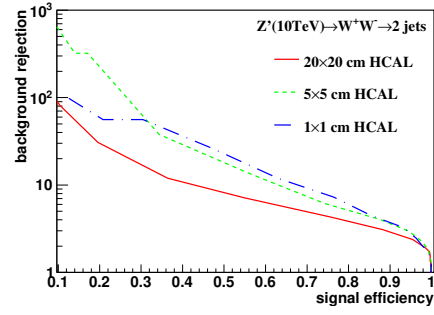


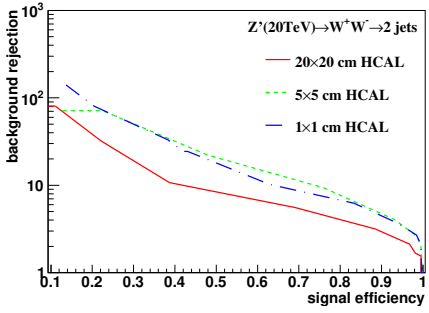
Figure 5: Distributions of Mann-Whitney value U in 5, 10, 20, 40TeV energy collision for c2b1 in different detector sizes. Cell Size in 20×20, 5×5, and 1×1(cm×cm) are shown here.



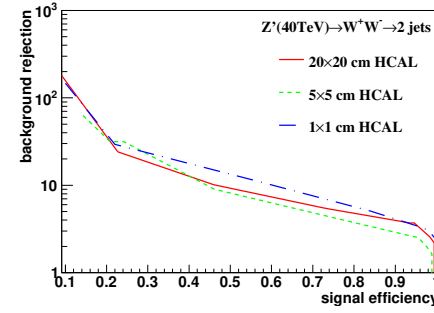
(a) 5 TeV using Rawhit 0.25GeV cut method with New2 after cut Method



(b) 10 TeV using Rawhit 0.25GeV cut method with New2 after cut Method



(c) 20 TeV using Rawhit 0.25GeV cut method with New2 after cut Method



(d) 40 TeV using Rawhit 0.25GeV cut method with New2 after cut Method

Figure 6: Signal efficiency versus background rejection rate using c2b1The energies of collision at (a)5, (b)10, (c)20, (d)40TeV are shown here. In each picture, the three ROC curves correspond to different detector sizes.

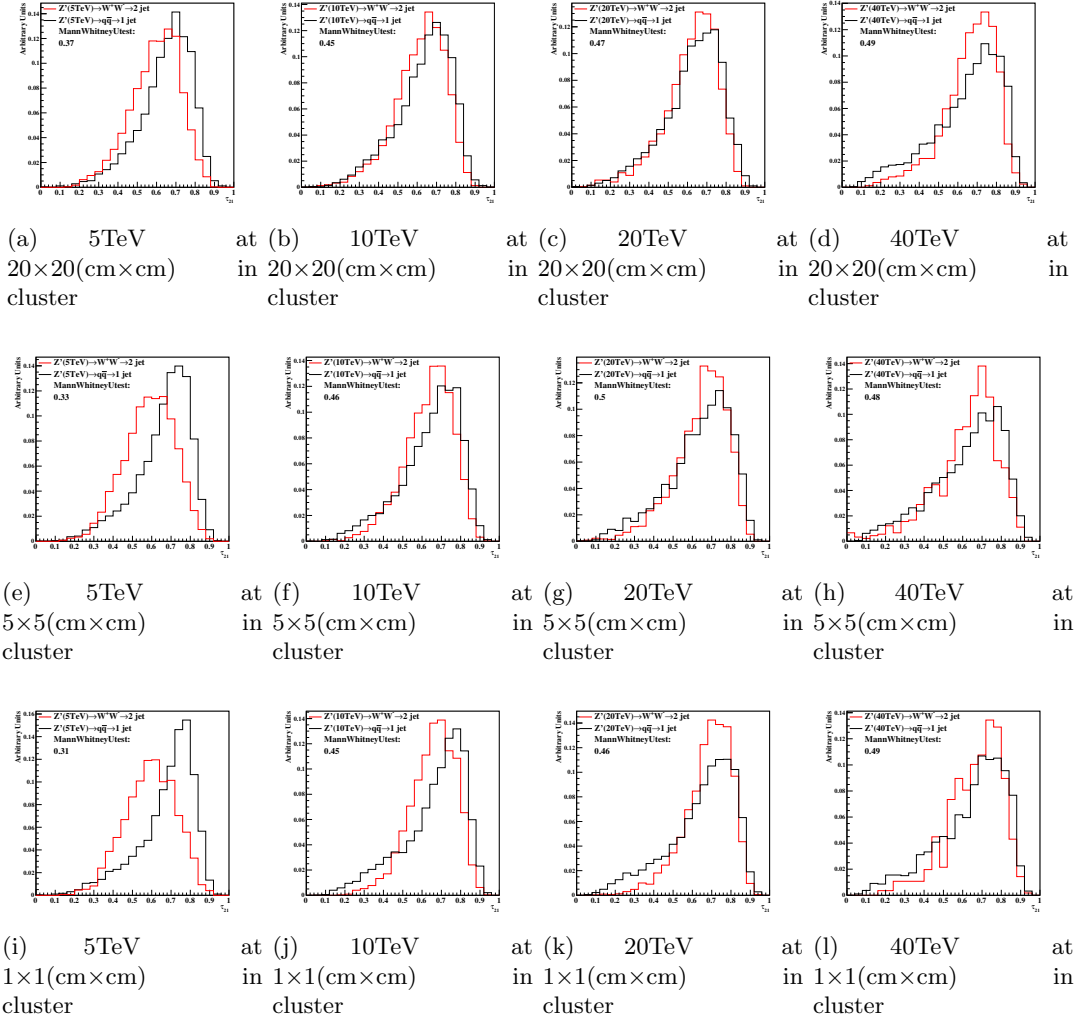
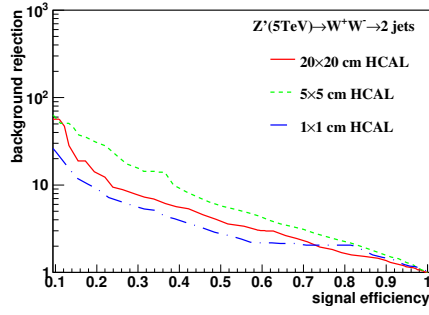
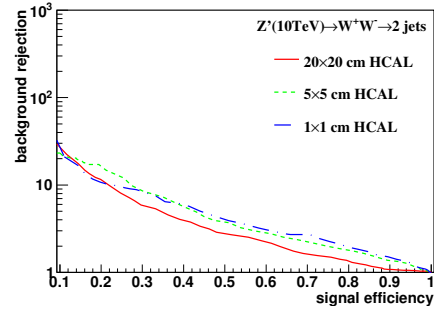


Figure 7: Distributions of Mann-Whitney value  $U$  in 5, 10, 20, 40 TeV energy collision for  $\tau_{21}$  in different detector sizes. Cell Size in 20x20, 5x5, and 1x1(cm x cm) are shown here.

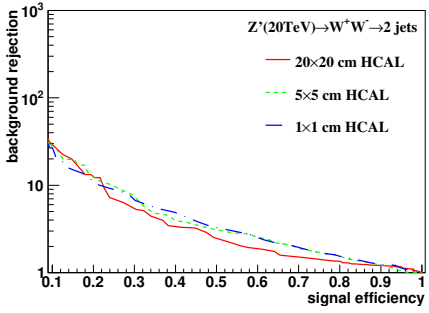




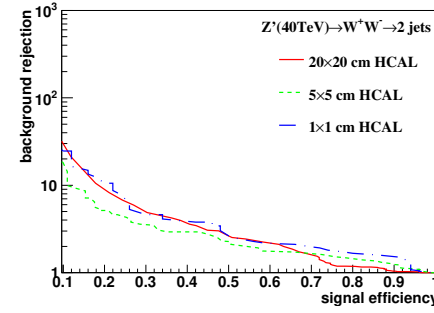
(a) 5 TeV using cluster method with New2 after cut Method



(b) 10 TeV using cluster method with New2 after cut Method



(c) 20 TeV using cluster method with New2 after cut Method



(d) 40 TeV using cluster method with New2 after cut Method

Figure 8: Signal efficiency versus background rejection rate using  $\tau_{21}$ . The energies of collision at (a)5, (b)10, (c)20, (d)40TeV are shown here. In each picture, the three ROC curves correspond to different detector sizes.

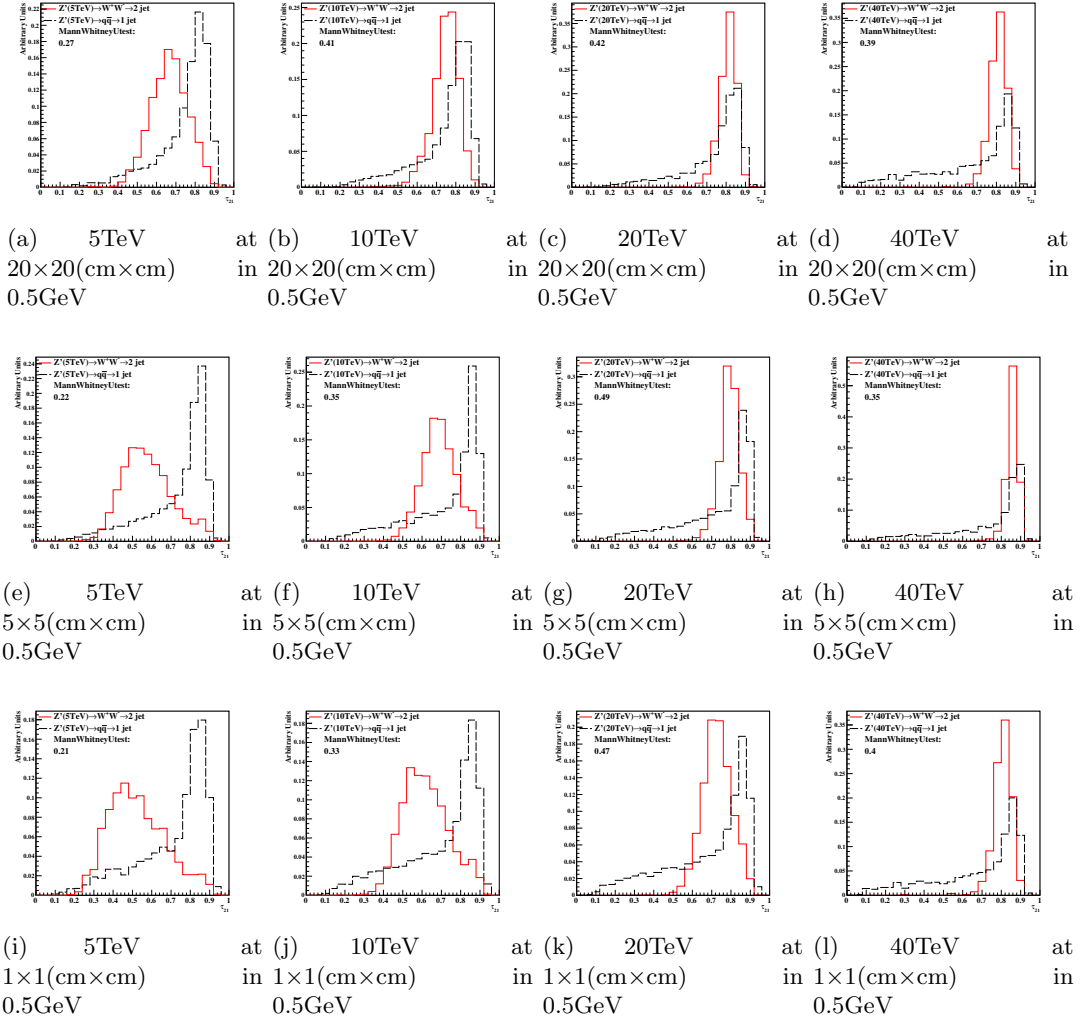
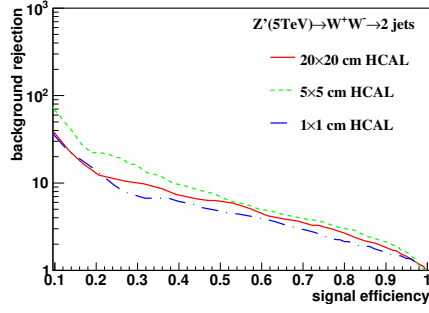
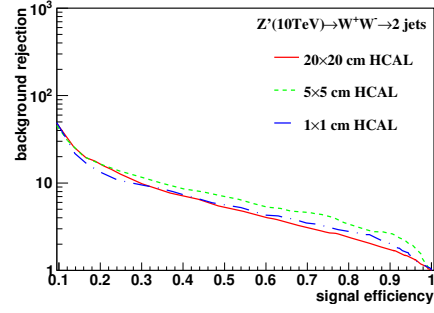


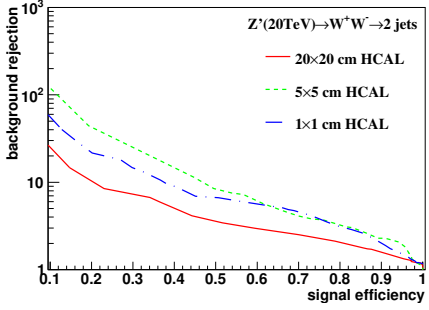
Figure 9: Distributions of Mann-Whitney value U in 5, 10, 20, 40TeV energy collision for  $\tau_{21}$  in different detector sizes. Cell Size in 20 $\times$ 20, 5 $\times$ 5, and 1 $\times$ 1(cm $\times$ cm) are shown here.



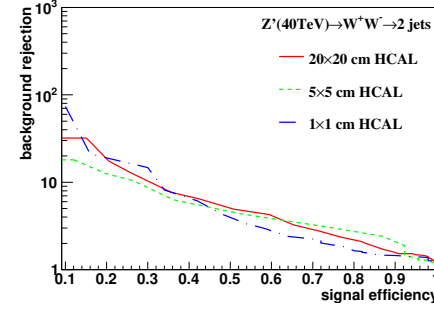
(a) 5 TeV using Rawhit 0.5GeV cut method with New2 after cut Method



(b) 10 TeV using Rawhit 0.5GeV cut method with New2 after cut Method



(c) 20 TeV using Rawhit 0.5GeV cut method with New2 after cut Method



(d) 40 TeV using Rawhit 0.5GeV cut method with New2 after cut Method

Figure 10: Signal efficiency versus background rejection rate using  $\tau_{21}$ . The energies of collision at (a)5, (b)10, (c)20, (d)40TeV are shown here. In each picture, the three ROC curves correspond to different detector sizes.

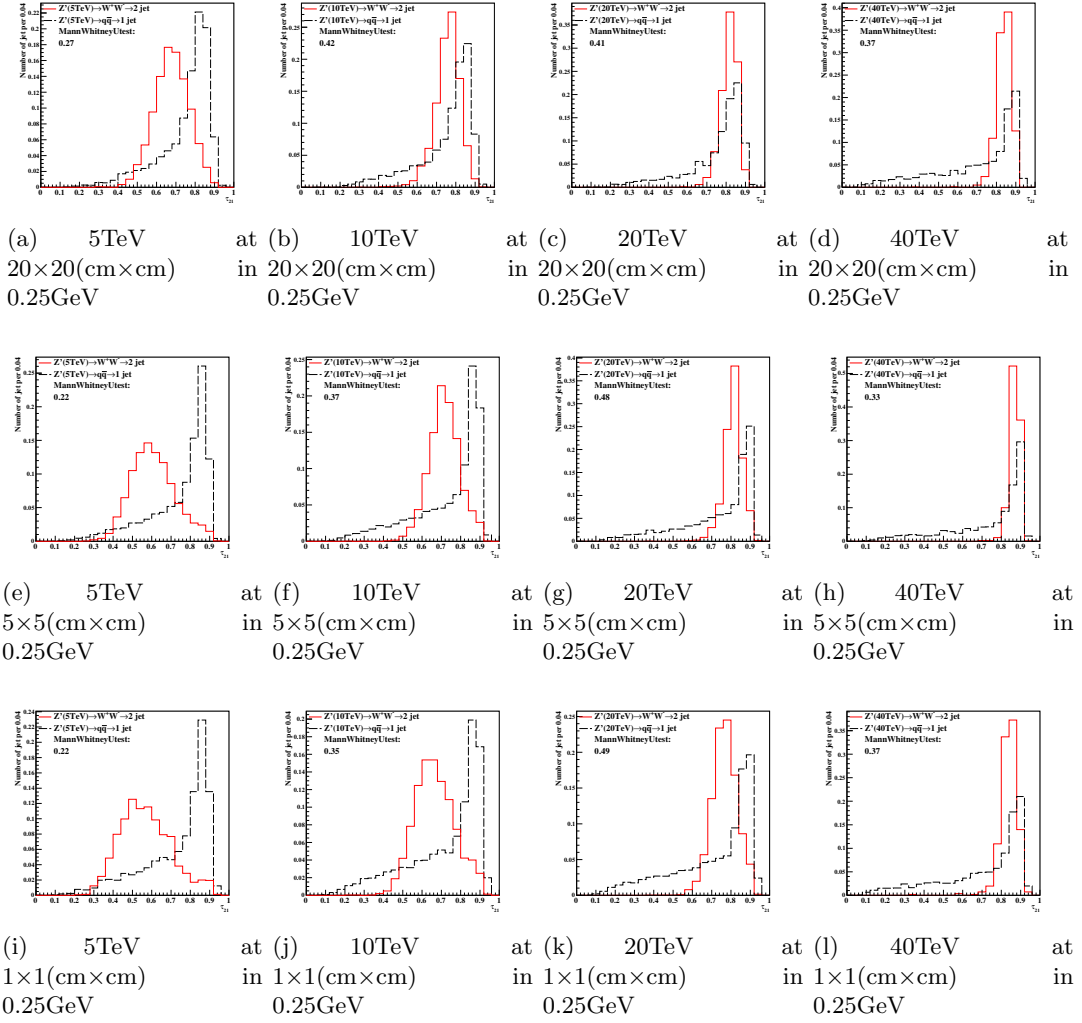
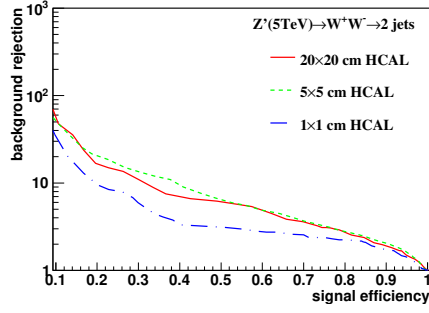
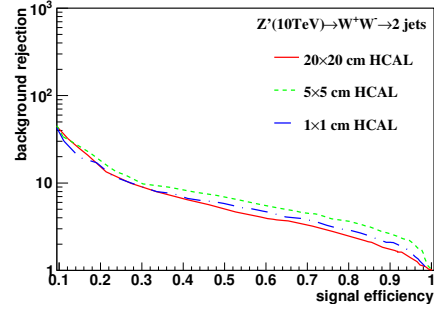


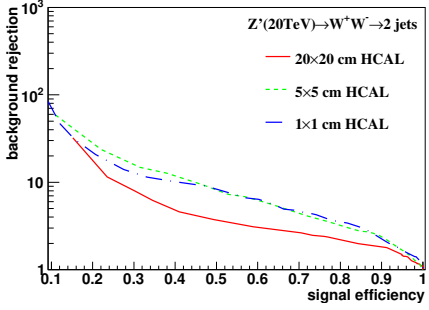
Figure 11: Distributions of Mann-Whitney value  $U$  in 5, 10, 20, 40TeV energy collision for  $\tau_{21}$  in different detector sizes. Cell Size in 20x20, 5x5, and 1x1(cm×cm) are shown here.



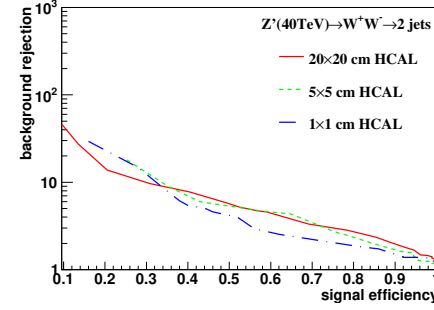
(a) 5 TeV using Rawhit 0.25GeV cut method with New2 after cut Method



(b) 10 TeV using Rawhit 0.25GeV cut method with New2 after cut Method



(c) 20 TeV using Rawhit 0.25GeV cut method with New2 after cut Method



(d) 40 TeV using Rawhit 0.25GeV cut method with New2 after cut Method

Figure 12: Signal efficiency versus background rejection rate using  $\tau_{21}$ . The energies of collision at (a)5, (b)10, (c)20, (d)40TeV are shown here. In each picture, the three ROC curves correspond to different detector sizes.

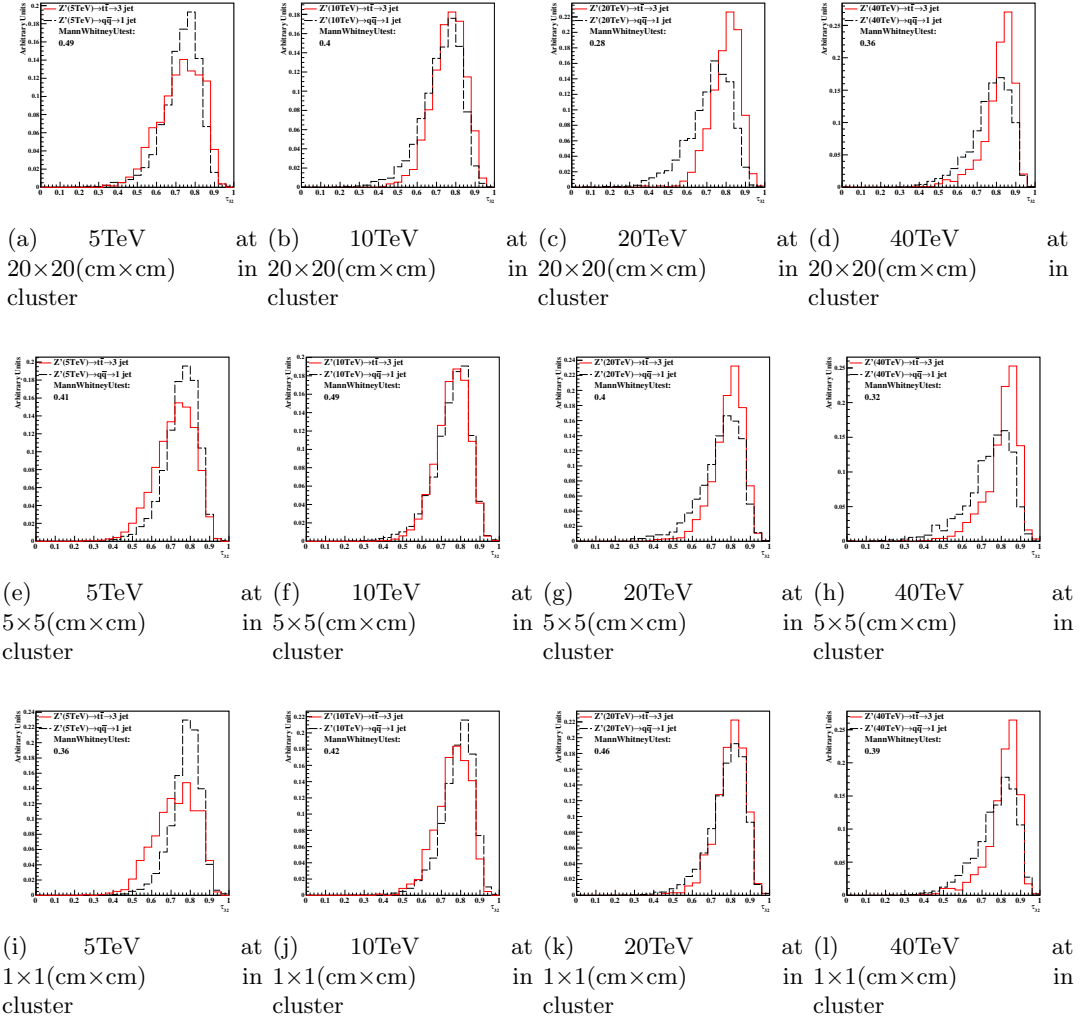
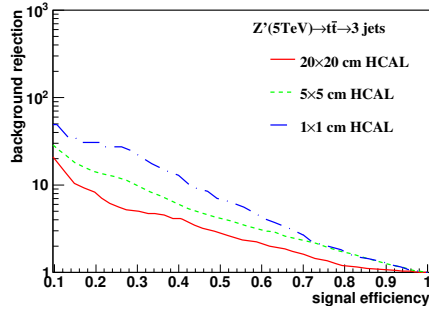
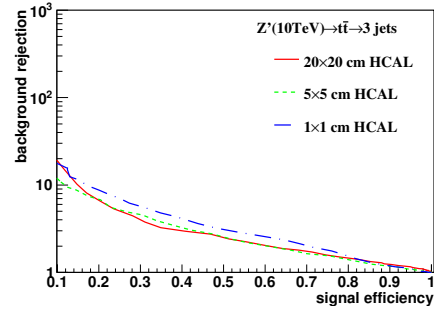


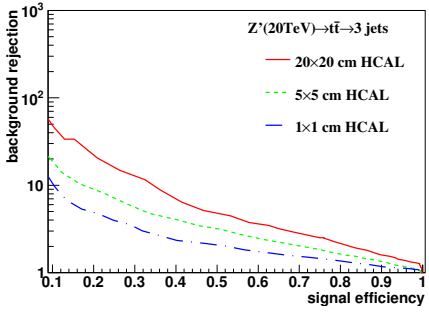
Figure 13: Distributions of Mann-Whitney value  $U$  in 5,10,20,40TeV energy collision for  $\tau_{32}$  in different detector sizes. Cell Size in 20 $\times$ 20, 5 $\times$ 5, and 1 $\times$ 1(cm $\times$ cm) are shown here.



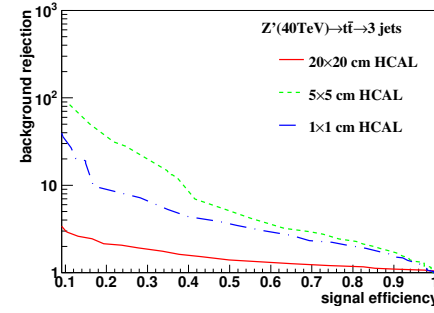
(a) 5 TeV using cluster method with New2 after cut Method



(b) 10 TeV using cluster method with New2 after cut Method



(c) 20 TeV using cluster method with New2 after cut Method



(d) 40 TeV using cluster method with New2 after cut Method

Figure 14: Signal efficiency versus background rejection rate using  $\tau_{32}$ . The energies of collision at (a)5, (b)10, (c)20, (d)40TeV are shown here. In each picture, the three ROC curves correspond to different detector sizes.

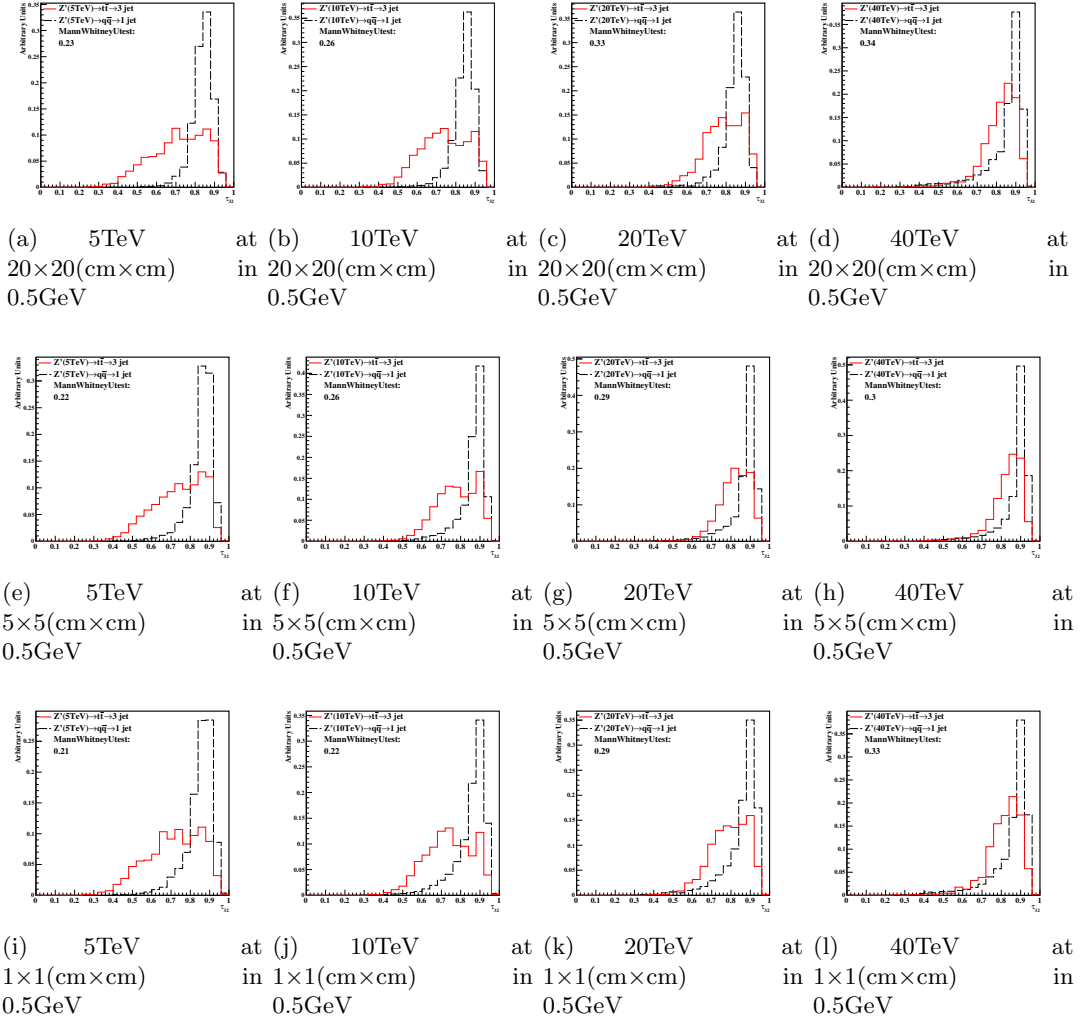
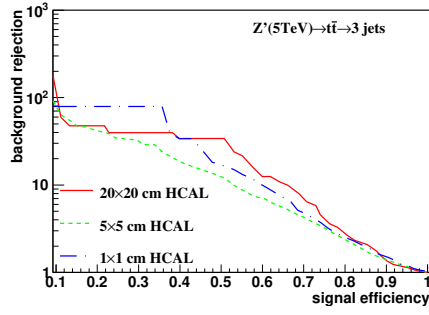
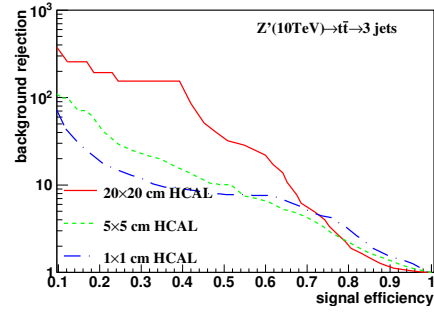


Figure 15: Distributions of Mann-Whitney value  $U$  in 5, 10, 20, 40TeV energy collision for  $\tau_{32}$  in different detector sizes. Cell Size in 20 $\times$ 20, 5 $\times$ 5, and 1 $\times$ 1(cm $\times$ cm) are shown here.

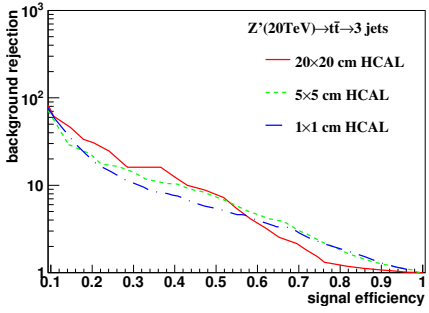




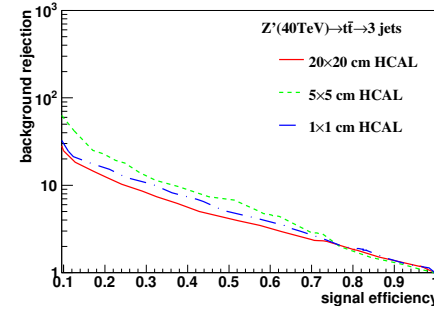
(a) 5 TeV using Rawhit 0.5GeV cut method with New2 after cut Method



(b) 10 TeV using Rawhit 0.5GeV cut method with New2 after cut Method



(c) 20 TeV using Rawhit 0.5GeV cut method with New2 after cut Method



(d) 40 TeV using Rawhit 0.5GeV cut method with New2 after cut Method

Figure 16: Signal efficiency versus background rejection rate using  $\tau_{32}$ . The energies of collision at (a)5, (b)10, (c)20, (d)40TeV are shown here. In each picture, the three ROC curves correspond to different detector sizes.

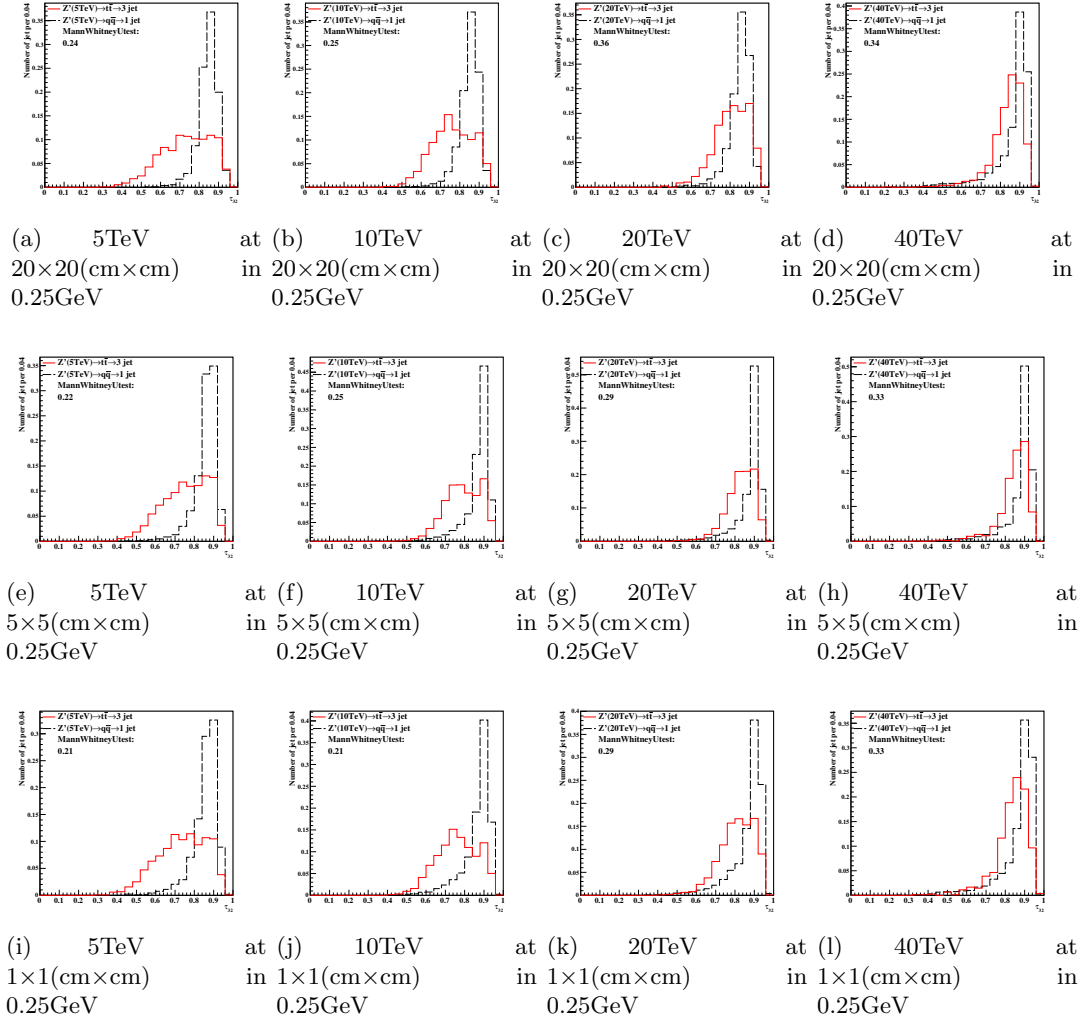
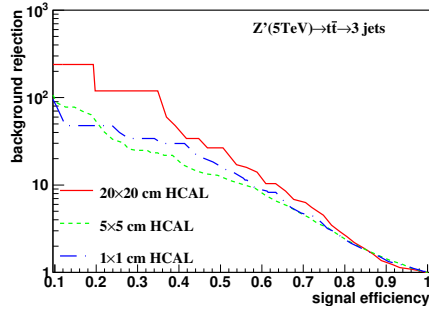
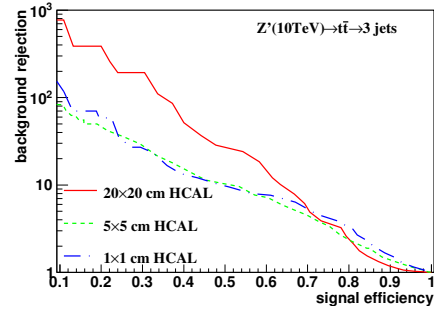


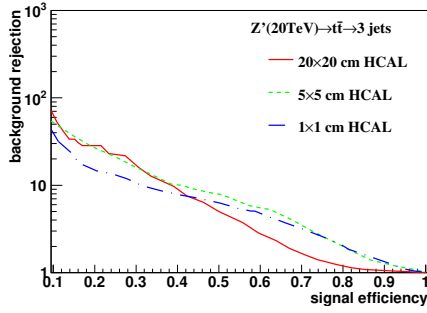
Figure 17: Distributions of Mann-Whitney value  $U$  in 5, 10, 20, 40TeV energy collision for  $\tau_{32}$  in different detector sizes. Cell Size in 20 $\times$ 20, 5 $\times$ 5, and 1 $\times$ 1(cm $\times$ cm) are shown here.



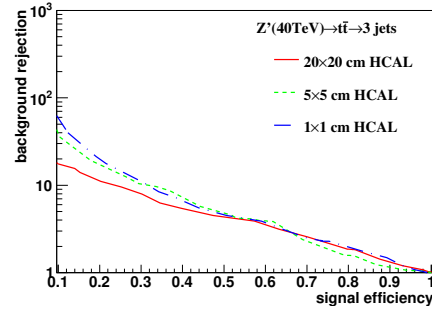
(a) 5 TeV using Rawhit 0.25GeV cut method with New2 after cut Method



(b) 10 TeV using Rawhit 0.25GeV cut method with New2 after cut Method

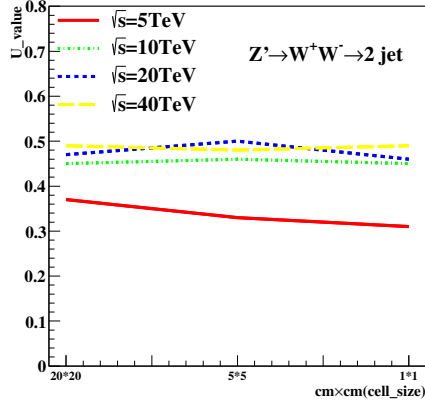


(c) 20 TeV using Rawhit 0.25GeV cut method with New2 after cut Method

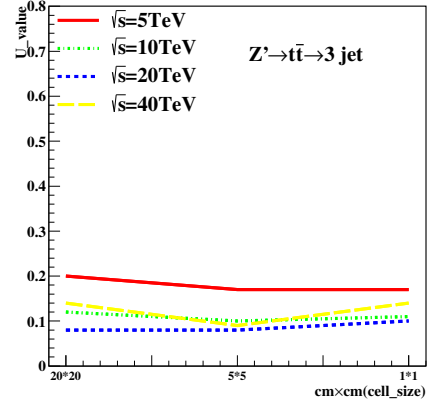


(d) 40 TeV using Rawhit 0.25GeV cut method with New2 after cut Method

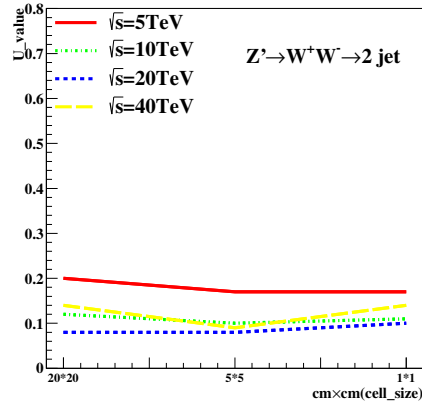
Figure 18: Signal efficiency versus background rejection rate using  $\tau_{32}$ . The energies of collision at (a)5, (b)10, (c)20, (d)40TeV are shown here. In each picture, the three ROC curves correspond to different detector sizes.



(a)  $\tau_{21}$  in cluster

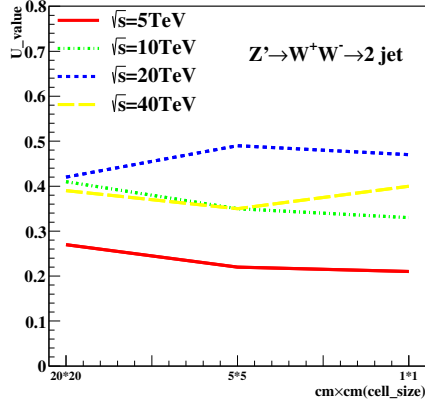


(b)  $\tau_{32}$  in cluster

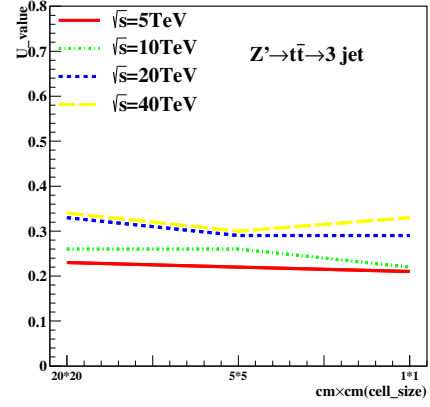


(c)  $c_2^{(1)}$  in cluster

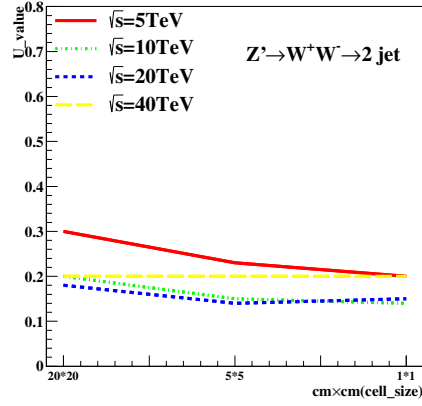
Figure 19: The Mann-Whitney U values for  $\tau_{21}, \tau_{32}$  and  $c_2^{(1)}$  reconstructed from calorimeter clusters at different collision energies correspond to different detector sizes in cluster. The energies of collision at 5, 10, 20, 40, 20, 40TeV are shown in each figure.



(a)  $\tau_{21}$  rawhit cut at 0.5 GeV

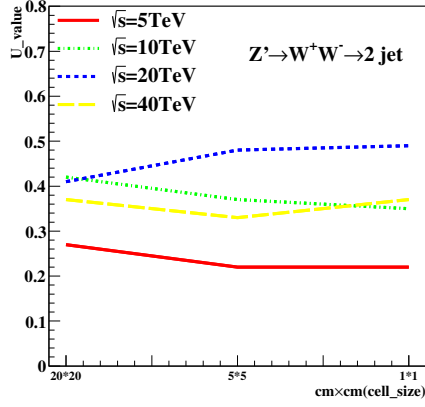


(b)  $\tau_{32}$  rawhit cut at 0.5 GeV

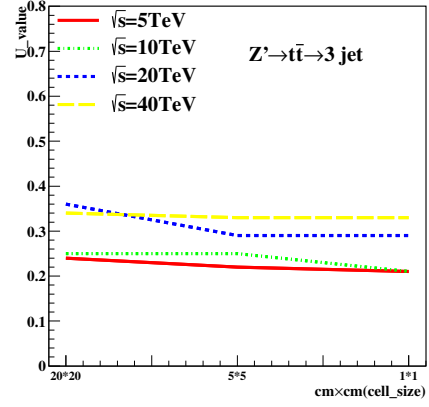


(c)  $c_2^{(1)}$  rawhit cut at 0.5 GeV

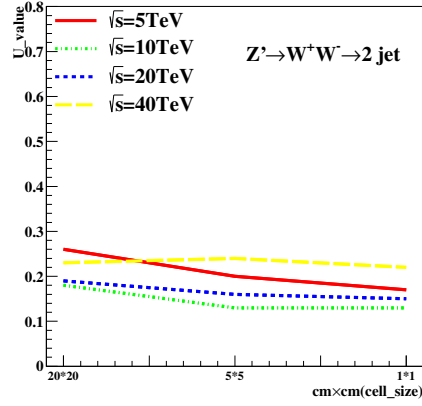
Figure 20: The Mann-Whitney U values for  $\tau_{21}, \tau_{32}$  and  $c_2^{(1)}$  reconstructed from calorimeter hit at 0.5 GeV cut at different collision energies correspond to different detector sizes in rawhit cut at 0.5 GeV. The energies of collision at 5, 10, 20, 40, 20, 40 TeV are shown in each figure.



(a)  $\tau_{21}$  rawhit cut at 0.25GeV



(b)  $\tau_{32}$  rawhit cut at 0.25GeV



(c)  $c_2^{(1)}$  rawhit cut at 0.25GeV

Figure 21: The Mann-Whitney U values for  $\tau_{21}, \tau_{32}$  and  $c_2^{(1)}$  reconstructed from calorimeter hit at 0.25GeV cut at different collision energies correspond to different detector sizes in cluster. The energies of collision at 5, 10, 20, 40, 20, 40TeV are shown in each figure.